PAPER

Check for updates

Metal–organic frameworks loaded Au nanozymes with enhanced peroxidase-like activity for multi-targeted biodetection†

Quan Liu,[ab] Hanhan Wang,[b] Qi Yang,*[a] Yuping Tong*[b] and Weiwei He [ID] [a]

Size and surface effects definitely play an important role in promoting the enzyme-like catalytic activity of metal nanozymes. However, monodisperse small-size nanozymes require surface modification to avoid agglomeration, which largely limits their catalytic activity. In this work, a zirconium-based metal organic framework (UiO-66) with high chemical stability and porosity was applied as a carrier, on which uniform Au nanoparticles (NPs) were successfully loaded, forming Au/UiO-66 nanocomposites. Benefiting from the naked and active surface of the distributed Au NPs, Au/UiO-66 exhibited prominently enhanced peroxidase activity as well as good performance and stability. Inspired by the significant peroxidase activity of Au/UiO-66 and the distinct inhibitory effect of biological substances on peroxidase activity, a multi-targeted analytical platform was designed and established. The results proved that the developed platform realized accurate and effective detection for glucose, dopamine and HS⁻ with a limit of detection (LOD) of 0.033 mM, 0.0022 mM and 0.0016 mM, respectively.

1. Introduction

The dynamic balance of biomolecules is vital for maintaining the health of the human body.[1] For example, glucose is an indispensable substance and energy in metabolism[2] and abnormal fluctuations in glucose will dramatically affect health.[3–5] Dopamine (DA) is an important neurotransmitter in the human brain and body.[6] DA deficiency and flooding have been linked to diseases and behaviors such as Parkinson's disease, attention deficit hyperactivity disorder, Alzheimer's disease, and addiction.[7–9] Endogenous H_2S, along with two other important endogenous gases, nitric oxide (NO) and (carbon monoxide) CO, have extensive physiological effects on the central nervous system, respiratory system, and cardiac system.[10–15] The efficient detection of such biologically active substances is important for

medical diagnosis and health monitoring.[16] In recent years, many detection methods have been applied for the detection of biomolecules such as electrochemical and fluorescence techniques. However, most of these detection methods require relatively expensive equipment and some biomolecular signals may interfere with each other.[17,18] For example, the electrochemical response to DA can easily be affected by ascorbic acid (AA), uric acid (UA), and other biomolecules due to their close oxidation potentials.[19] Specific colorimetric detection based on enzyme catalysis could largely alleviate these problems, and the detection target is relatively specific. For the rapid screening of health and diseases, it is essential to develop a detection platform for biologically active substances with accurate and multi-targeted function.

With the remarkable development of nanotechnology, nanozymes have emerged as a hot topic and have received extensive consideration because of their unique advantages.[20–23] In particular, their excellent biological activity and safety mean nanozymes have excellent application prospects in the biomedical field.[24–27] In nanozyme-enabled analytical chemistry,[28,29] the outstanding peroxidase-like activity is proposed to detect a great number of biological substances *in vivo* and *in vitro*, especially for biomolecules.[30,31] Among the hundreds of nanozymes, noble metal based nanozymes have the advantages of a clear and adjustable structure, easy surface modification, and good biocompatibility.[32] The implementation of nanozymes in biological analysis largely relies on their high catalytic efficiency and stability. Most studies have shown that small-size

[a] *Key Laboratory of Micro-Nano Materials for Energy Storage and Conversion of Henan Province, Institute of Surface Micro and Nano Materials, College of Chemical and Materials Engineering, Xuchang University, Xuchang, Henan 461000, P. R. China. E-mail: yangq@xcu.edu.cn*

[b] *School of Materials, North China University of Water Resources and Electric Power, Zhengzhou, Henan 450045, China. E-mail: yptong_zz@163.com*

† Electronic supplementary information (ESI) available: SEM images of UiO-66 (a and b) and Au/UiO-66 nanocomposites (c and d) (Fig. S1); N_2 absorption–desorption isotherms of UiO-66 and Au/UiO-66 (Fig. S2); XRD patterns of pure UiO-66 and Au/UiO-66 nanocomposites (Fig. S3); UV-Vis absorption spectra of UiO-66/TMB in the presence and absence of H_2O_2 (Fig. S4). A comparison of the absorption spectra of Au/UiO-66 and Pt/UiO-66 oxidase-like and interference degree of specific detection (Fig. S5). A comparison of the kinetic parameters among the nanozymes (Table S1). See DOI: https://doi.org/10.1039/d2ma00844k

noble metal NPs exhibit higher catalytic activity due to exposure to more active sites and large specific surface areas.[33,34] However, small-size noble metal NPs usually need surface modification to overcome the agglomeration effect, which largely limits their catalytic activity.[35] Therefore, rational designs of nanozyme containing small-size, clean-surface noble NPs need to be explored for sensitive and multi-targeted detection purposes.

Metal–organic frameworks (MOFs), structured from organic ligands and inorganic metal ions, are a series of interesting materials with outstanding crystallinity, diverse structures, large surface areas, good adsorption performance, and excellent component tunability.[36–38] MOFs could be recognized as an appropriate carrier for metal NPs. Loaded metal NPs are possibly evenly distributed on the surface or in the interstitial space of MOFs, which could effectively avoid agglomeration and elevate their catalytic activity as well as stability. UiO-66, one of the representatives of MOF materials, is notable for its good stability and has been proposed in several studies in biological applications.[38–42]

In this work, a zirconium-based metal organic framework (UiO-66) with high chemical stability and porosity was applied as a carrier, on which small and uniformly distributed Au NPs were successfully loaded, forming a new nanocomposite (Au/UiO-66). The pH and temperature stability of Au/UiO-66 were evaluated. The peroxidase-like activity was tested and compared with that of commercial 5 nm Au spheres. Using the enhanced peroxidase-like activity of Au/UiO-66, a multi-targeted detection system was developed based on a distinct mechanism, which aimed to realize the accurate and effective detection of glucose, dopamine and HS⁻.

2. Experimental section

2.1. Chemical and materials

Zirconium tetrachloride ($ZrCl_4$), 1,4-benzenedicarboxylic acid (H_2BDC), N,N'-dimethylformamide (DMF), acetic acid, absolute ethanol, chloroauric acid ($HAuCl_4$), sodium borohydride ($NaHB_4$), 3,3′,5,5′-tetramethylbenzidine (TMB), o-phenylenediamine (OPD), hydrogen peroxide (H_2O_2), dopamine (DA) and sulfur sodium hydride (NaHS) were analytically purified and were purchased from Sinopharm Chemical Reagent Co. Ltd (Beijing, China). The 5 nm Au nanospheres were purchased from Nanocomposix. Glucose came from Kaitong Chemical Reagent Co. (Tianjin, China). Glucose oxidase (from *Aspergillus niger*, GOx) is commercially available from Aladdin Industrial Co. (CA, USA). Milli-Q water (18 MΩ cm) was used for all the experimental preparations. All glassware and the autoclave used in the following procedures were cleaned by aqua regia solution ($HNO_3/HCl = 1:3$ v/v).

2.2. Synthesis of Au/UiO-66 nanocomposites

The preparation process of the Au/UiO-66 nanocomposites can be divided into two steps. In the first step, the carrier UiO-66 material was prepared according to the previous method. 116.6 mg of $ZrCl_4$ (0.5 mmol) and 83.1 mg of H_2BDC (0.5 mmol) were respectively dissolved in 10 mL of DMF and then mixed with

4 mL acetic acid. The solution was stirred magnetically for 20 minutes at room temperature and then transferred to a 50 mL stainless steel autoclave lined with Teflon, and then sealed and placed in an oven at 180 °C for 5 h. After cooling to room temperature, the white precipitate was collected and washed by centrifugation, once with DMF and three times with absolute ethanol. The UiO-66 was dried in a vacuum cabinet at 60 °C for further use.

In the second step, Au/UiO-66 nanocomposites were prepared by a chemical reduction method. 9.4 mg UiO-66 was dispersed in 3 mL anhydrous ethanol and ultrasonically stirred until the solution was uniform. 125 μL of 24 mM $HAuCl_4$ was added and stirred at room temperature for more than 6 hours. Then the solution was dispersed into 3 mL of anhydrous ethanol. After that, 120 μL of 0.5 M $NaBH_4$ was added to the above solution at room temperature to reduce Au^{3+}. In order to make the grain size of Au NPs more uniform, the injection pump was used to evenly add $NaBH_4$ solution at the rate of 4 μL min⁻¹. The reaction time was 1.5 hours.

After the reaction, the purplish red precipitate was collected by centrifugation. Then the collected precipitate was washed once with ethanol, twice with deionized water and kept in a constant volume of 2 mL for further use. After the above process, Au/UiO-66 nanocomposites were obtained with an Au loading capacity of about 6%.

2.3. Characterization

Scanning electron microscope (SEM) images were captured using a FEI Nova 450 field emission electron microscope. X-ray diffractometry (XRD, Bruker D8) was used to collect X-ray diffraction patterns using monochrome Cu Kα radiation ($\lambda = 1.5418$ Å). Transmission electron microscopy (TEM) images were taken on a Tecnai G2 F20 U-Twin electron microscope with an accelerated voltage of 200 kV. That same microscope was used to perform dark field imaging, EDS mapping, and high-resolution TEM (HRTEM). UV-Visible absorption spectra were obtained by a UV-Vis-NIR Spectrometer (Varian Cary 5000). N_2 adsorption and desorption curves were obtained by Micromeritics Instrument Corporation ASAP 2020 V4.00 and the desorption temperature and time were set to 150 °C for 8 hours. X-ray photoelectron spectroscopy (XPS) was performed with a Thermo ESCALAB 250XI multifunctional imaging electron spectrometer (Thermo Fisher Scientific, USA) using 150 W Al Kα radiation and a base pressure of approximately 3×10^{-9} mbar. The binding energies were calibrated to the C 1s line at 284.8 eV.

2.4. Measurement of the peroxidase-like activity of Au/UiO-66 nanocomposites

The peroxidase-like activity of Au/UiO-66 nanocomposites was investigated by catalyzing the oxidation of TMB with H_2O_2. Firstly, 20 μL of 20 mM TMB and 20 μL of 0.1 M H_2O_2 were mixed in 3 mL HAc–NaAc buffer (10 mM, pH = 6), and then 30 μL of 10.0 mg mL⁻¹ UiO-66 or Au/UiO-66 was added to start the catalytic oxidation of TMB. The color changes during TMB oxidation were monitored by UV-Vis absorption spectroscopy. The scanning kinetic model was used to record the absorption

spectra every 2 min and analyze the kinetics of TMB catalytic oxidation reaction. In order to confirm the accuracy of the experimental results, the color developer TMB was changed with OPD, whose testing results also supported the good peroxidase-like activity of Au/UiO-66. As a control, the same method was also applied to evaluate the peroxidase- and oxidase-like activity of commercial 5 nm Au spheres protected by surfactant PVP.

The apparent steady-state kinetic measurements of dynamics were carried out for different Au/UiO-66 nanostructures. The parameters were calculated based on the Michaelis–Menten equation:

$$1/\nu = (K_m/V_{max}) \times (1/[S]) + 1/V_{max}$$

where ν is the reaction initial velocity, V_{max} is the maximal reaction velocity, [S] is the concentration of substrate and K_m is the Michaelis constant.

2.5. Detection of glucose

Glucose concentration was detected based on the outstanding peroxidase-like activity of Au/UiO-66. 480 μL glucose aqueous solution and 40 μL of 100 U mL^{-1} glucose oxidase were taken and reacted at 37 °C for 30 min. Then 2.5 mL HAc–NaAc buffer containing 20 μL of 20 mM TMB (10 mM, pH = 6.0) was added. The discoloration reaction was triggered by adding 30 μL of 5 mg mL^{-1} Au/UiO-66 suspension. At 37 °C for 15 minutes, the UV-Vis absorption spectra were analyzed. In order to determine the selectivity of this method for glucose detection, we also replaced glucose with other sugars, such as maltose, galactose, fructose and sucrose, whose concentration was 1 mM. All other reaction conditions remained unchanged. The UV-Vis absorption spectrum was used to test the concentration samples 21 times, and the standard deviation of the blank samples was obtained. The slope was obtained by linear fitting of absorption intensity and glucose concentration at 650 nm. The detection limit is obtained by the following formula:

$$\text{LOD} = \frac{3\delta}{k}$$

where δ is the standard deviation of blank measurement and k is the slope between the absorbance intensity *versus* glucose.

2.6. Detection of dopamine

Dopamine concentration was measured based on the reduction reaction, in which dopamine consumes H_2O_2 and produces dopamine-*o*-quinine. Firstly, x μL of 2 mM dopamine solution was added to 2930-x μL (x = 0, 10, 20, 40, 60, 80, and 100) deionized water, respectively. Then 20 μL of 20 mM TMB and 20 μL of 0.1 M H_2O_2 were added to the solution. Finally, 30 μL 5 mg mL^{-1} Au/UiO-66 suspension was added and reacted at 30 °C for 15 minutes. UV-Vis absorption spectra were recorded.

2.7. Detection of HS$^-$

The concentration of HS$^-$ was detected based on the remarkable inhibiting effect of HS$^-$ on the peroxidase-like activity of Au/UiO-66. Firstly, x μL of 2 mM NaHS solution was added to 2930-x μL (x = 0, 2.5, 5, 7.5, 10, 20, 30, and 40) deionized water, respectively.

Then 20 μL of 20 mM TMB and 20 μL of 0.1 M H_2O_2 were added to the solution. Finally, 30 μL of 5 mg mL^{-1} Au/UiO-66 suspension was added and reacted at 30 °C for 15 minutes. UV-Vis absorption spectra were recorded. In order to determine the selectivity for the detection of HS$^-$, we used other ions to replace HS$^-$, such as K$^+$, Na$^+$, Mg^{2+}, Mn^{2+}, Ni$^+$, Co^{2+}, Zn^{2+}, Cu^{2+} and Ca^{2+}, at a concentration of 10 mM and with glycine (Gly), glutathione (GSH) and S^{2-} at a concentration of 2 mM. All other reaction conditions remained unchanged.

3. Results and discussion

3.1. Formation and characterization of the Au/UiO-66 nanocomposites

Firstly, UiO-66 was synthesized through hydrothermal treatment of zirconium tetrachloride, terephthalic acid (H$_2$BDC) and acetic acid under 180 °C (Fig. 1a). The synthesized UiO-66 has good dispersion, a clean surface and uniform particle size, with an average particle size of about 500 nm (Fig. 1b and c, Fig. S1a and b, ESI†). The Brunauer–Emmett–Teller (BET) surface area is measured to be ~1312.8 m^2 g^{-1} and the average pore size is 1.0179 nm (Fig. S2, ESI†). Au NPs are successfully loaded and uniformly distributed on the UiO-66 matrices, the particle size (diameter) of Au is calculated to be 7 ± 0.45 nm. The HRTEM of the selected Au particle reveals that the distance between adjacent lattices is about 0.235 nm (Fig. 1d and e), which is consistent with the planar distance of Au(111). After loading of the Au NPs, the specific surface area of Au/UiO-66 decreased to 328.8 m^2 g^{-1} and the pore volume decreased from 0.74 cm^3 g^{-1} to 0.34 cm^3 g^{-1}.
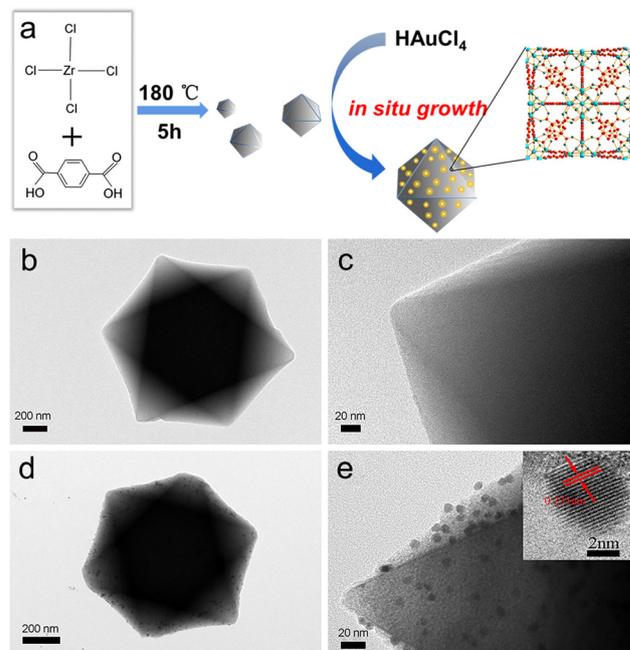

Fig. 1 The synthesis path diagram of the Au/UiO-66 composite structure (a); TEM images of different samples: (b) and (c) UiO-66 and (d) and (e) Au/UiO-66. The inset in (e) is a high-resolution image of the Au NPs.

The high angle annular dark field (HAADF) images and element mapping images of Au/UiO-66 are shown in Fig. 2. The representative element Au (Fig. 2c) and the constituent elements Zr, C, and O of UiO-66 (Fig. 2d–f) are uniformly distributed in the Au/UiO-66 nanocomposites. The observation and analysis results seem to confirm that Au NPs have been well loaded on the UiO-66 surface. Furthermore, the energy dispersive X-ray spectroscopy (EDS) results prove that the mass ratio of Au is 5.38 wt%, which agrees well with the calculated ratio (6%), indicating that the added Au^{3+} is completely reduced and combined with UiO-66.

The X-ray diffraction (XRD) patterns of pure UiO-66 and Au/UiO-66 nanocomposites are shown in Fig. S3 (ESI†). The strong diffraction peaks of carrier UiO-66 appear at $2\theta = 17.08°$, $22.25°$, $25.68°$ and $33.12°$, corresponding to the (004), (115), (224) and (137) crystal planes, respectively. Two additional diffraction peaks appear at $2\theta = 38.15°$ and $44.41°$ in Au/UiO-66, which correspond to the (111) and (200) crystal planes of Au. The low intensity of these two peaks is likely attributed to the low amount of loaded Au (6%). The XRD pattern of Au/UiO-66 is similar to that of pure UiO-66, which proves the structure of the UiO-66 remains unchanged after loading of Au NPs. The decrease of diffraction intensity is probably due to the large amount of Au NPs, which are uniformly distributed on the surface of UiO-66, reducing its exposed surface (Fig. S3, ESI†). X-ray photoelectron spectroscopy (XPS) spectra tests showed signals from Au 4f, Zr 3d, C 1s and O 1s (Fig. 3a), confirming the elementary composition of Au/UiO-66. By fitting the high-resolution XPS spectra of Au 4f (Fig. 3b), the double peaks of Au $4f_{7/2}$ (84.14 eV) and Au $4f_{5/2}$ (87.78 eV) could be confirmed as zero-valent Au (Au^0). However, the peaks of Au $4f_{5/2}$ at 88.64 eV

and Au $4f_{7/2}$ at 84.87 eV are fitted as Au^+, indicating that a small part of Au is in the oxide state.[43–45] The above data further prove the successful loading of Au on the carrier UiO-66.

3.2. Enhanced peroxidase-like activity of Au/UiO-66 nanocomposites

The peroxidase-like activity of Au/UiO-66 is evaluated by both TMB and OPD assays, which are typically chromogenic substrates. Fig. 4a shows clearly that Au/UiO-66 can efficiently catalyze the oxidation of TMB and OPD in the presence of H_2O_2 to produce a corresponding blue and yellow color with characteristic absorption in the visible region. In comparison, the control samples, in the absence of Au/UiO-66 or H_2O_2, show negligible color production and oxidation of TMB or OPD. This verifies that the Au/UiO-66 exhibits intrinsic peroxidase-like activity without any accompanying oxidase-like activity. It is reported that a variety of noble metal NPs (Pt, Au, Pd, Ru, Rh, *etc.*) often possess multiple enzyme-like activity, including peroxidase and oxidase.[46,47] The coexisting oxidase-like activity will generate an unsatisfactory background signal when using the peroxidase-like activity in the colorimetric detection of biological molecules (H_2O_2, glucose, cholesterol, *etc.*).[48] The unmodified UiO-66 did not show any peroxidase-like or oxidase-like activity (Fig. S4, ESI†). However, Au/UiO-66 nanocomposites have good peroxidase-like specificity (Fig. 4a), which can resolve the above problem and improve the signal to noise ratio. To demonstrate the enhanced peroxidase-like activity of Au/UiO-66, the catalytic activity of 5 nm Au spheres coated with PVP (Au@PVP) was evaluated and compared through TMB oxidation with H_2O_2. The amount of Au@PVP remained the same as the Au content in Au/UiO-66. The results exhibit that the catalytic activity of Au NPs on UiO-66 is about six times higher
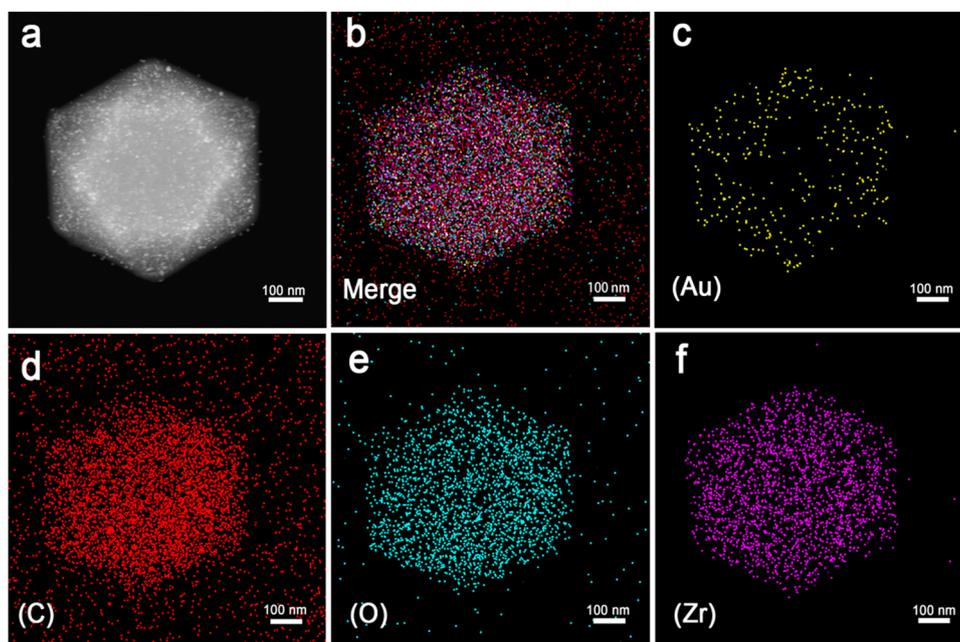

Fig. 2 The scanning TEM (STEM)–HAADF image of Au/UiO-66 (a) and STEM element mapping images of mixed elements (b) and Au (c), C (d), O (e), and Zr (f) of Au/UiO-66, respectively.
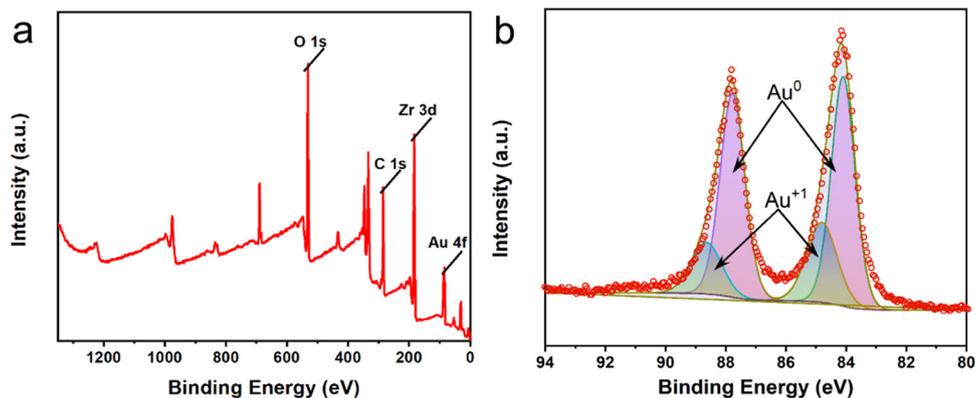
Fig. 3   (a) XPS survey of the Au/UiO-66 nanocomposites and (b) high-resolution spectra of Au 4f.
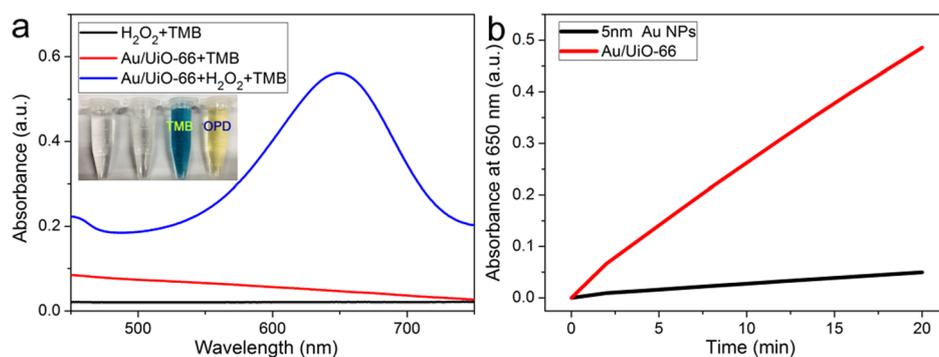

Fig. 4   (a) The reaction of Au/UiO-66 in different color-developing systems, the inset shows the photograph of different solutions (the reaction time is 20 min). (b) The absorbance at 650 nm as a function of reaction time, indicating reactions of 5 nm Au NPs and Au/UiO-66 with the solution containing TMB and H_2O_2.

than that of Au/PVP (Fig. 4b). Although the cladding of PVP effectively prevents the agglomeration of Au NPs, the catalytic activity is inescapably reduced. The loading of naked Au NPs on UiO-66 composites can provide a valuable strategy for solving the above problem. The carrier UiO-66 acts as an ideal host, providing sufficient active sites for Au NPs, which not only avoids agglomeration, but also guarantees the catalytic activity of the Au NPs.

Previous studies have proved that temperature and pH have significant effects on the activity of natural enzymes as well as

nanozymes.[49,50] Therefore, the effects of pH and temperature on the peroxidase activity of Au/UiO-66 were investigated. Reactions of TMB oxidation with H_2O_2 catalyzed by Au/UiO-66 were conducted. The peroxidase-like activity in the pH range of 2 to 10 was tested (Fig. 5a). Au/UiO-66 shows obvious pH-dependent catalytic activity, which increased with the increase of pH in strong acid conditions and decreased with the increase in pH in near neutral and weak alkaline conditions. The optimal pH value of Au/UiO-66 was about 6.0. It could be
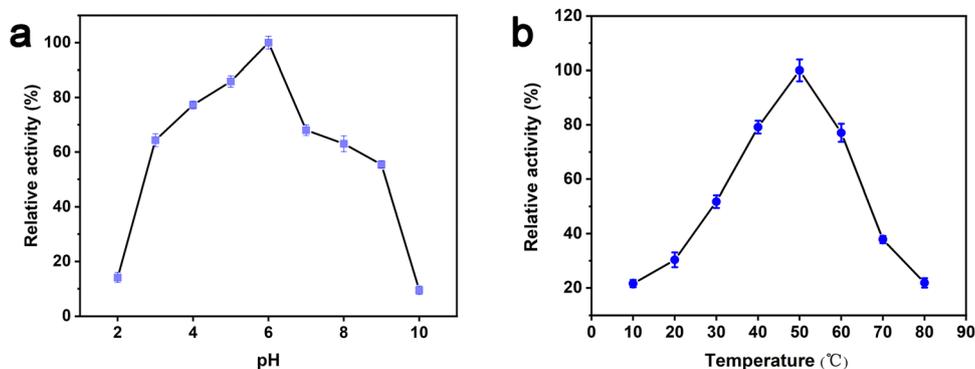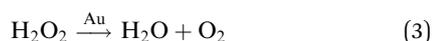

Fig. 5   Dependence of the Au/UiO-66 peroxidase-like activity on reaction conditions: (a) pH and (b) temperature.

observed in the experimental process that when TMB is added to the buffer solution close to neutral and weakly alkaline, a small amount of precipitate is generated, leading to the catalytic activity reduction of Au/UiO-66. Such a phenomenon can probably be ascribed to the diamine structure in TMB, which caused its poor solubility in weakly alkaline media.[46]

In order to investigate the influence of temperature on catalytic activity of Au/UiO-66, similar experiments were performed and the peak absorbance at 650 nm under 10–80 °C was also recorded (Fig. 5b). According to the experimental results, the optimal temperature range is 35–65 °C, revealing that Au/UiO-66 has a stable catalytic activity over a wide temperature range.

There are three different pathways for oxidation of TMB with H_2O_2 catalyzed by Au NPs. The first two pathways can accelerate the oxidation of color substrates (such as TMB and OPD), enhancing the peroxidase activity, while the third pathway can degrade H_2O_2 and slow down the oxidation of TMB,

$$H_2O_2 + 2HA \xrightarrow{Au} 2H_2O + 2A \quad (1)$$

$$H_2O_2 \xrightarrow{Au} 2 \bullet OH \quad (2)$$

$$H_2O_2 \xrightarrow{Au} H_2O + O_2 \quad (3)$$

Since pH can change the dissociation and standard reduction potential of H_2O_2, the oxidation/reduction capacity of H_2O_2 and its reaction pathway is greatly influenced by pH.[51,52] With the increase in pH value, the standard reduction

potential of H_2O_2 decreased, leading to the reduction of oxidation capacity. Therefore, the pathway 1 reaction was slowed down. At the same time, observation and analysis showed that under alkaline conditions with increasing pH, the pathway 3 reaction was triggered and H_2O_2 decomposed to oxygen and water, which further reduced its peroxidase-like catalytic activity.[53] In conclusion, the pH-dependent and peroxidase-like activity of Au/UiO-66 was attributed not only to the catalytic properties of Au NPs, but also to the pH-dependent physical and chemical properties of the reactant substrates (TMB and H_2O_2).

The Michaelis–Menten constant (K_m) and the maximal reaction velocity (V_{max}) of TMB oxidation were calculated through fitting the typical double reciprocal graph to the Michaelis–Menten model. K_m is the concentration of the substrate [S] when the enzymatic reaction reaches half of the V_{max}, which represents the affinity between the enzyme and the substrate. For natural enzymes, a small K_m generally means a high affinity and catalytic activity. Under the constant H_2O_2 concentration of 0.67 mM, the influence of TMB concentration on reaction rate of the Au/UiO-66 catalyzed oxidation was investigated (Fig. 6a). The Michaelis–Menten equation was applied to calculate the corresponding double reciprocal diagram of the enzyme kinetic parameters (Fig. 6b). When the reaction substrate was TMB, the calculated results were $K_m = 0.036$ mM and $V_{max} = 6.1 \times 10^{-8}$ M s^{-1} for Au/UiO-66. Furthermore, under the constant TMB concentration of 0.13 mM, the influence of H_2O_2 concentration on the reaction rate of the Au/UiO-66 catalyzed oxidation is shown in Fig. 6c. The corresponding double reciprocal diagram of
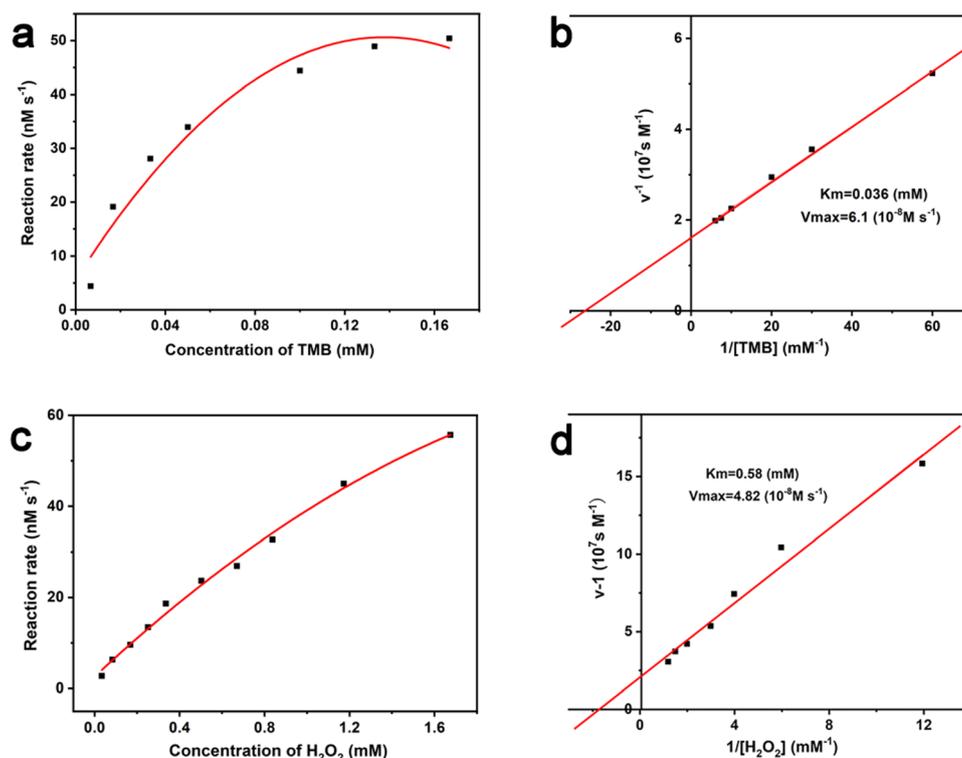

Fig. 6 (a) Effect of TMB concentration on the Au/UiO-66 catalytic oxidation TMB reaction rate. (b) The corresponding double reciprocal graph of (a). (c) The effect of H_2O_2 concentration on the reaction rate of Au/UiO-66 catalyzed TMB oxidation. (d) The corresponding double reciprocal graph of (c).

the enzyme kinetic parameters was also characterized using the Michaelis–Menten model (Fig. 6d). The K_m and V_{max} for Au/UiO-66 were calculated to be 0.58 mM and 4.82×10^{-8} M s^{-1}, respectively. These results demonstrate that the reaction rate gradually increased with the rising concentration of TMB or H_2O_2 until it reached the maximum value. The kinetic parameters of Au/UiO-66 were compared with those of natural horseradish peroxidase (HRP) and other Au-based nanozymes (Table S1, ESI†). The results showed that Au/UiO-66 has an outstanding affinity and higher catalytic rate.

3.3. Detection of glucose, dopamine and bisulfide based on the peroxidase-like activity of Au/UiO-66 nanocomposites

H_2O_2 is the oxidation product of many biomolecules. A striking example closely related to health is the oxidation of glucose, generating gluconic acid and H_2O_2. In recent years, the effective cascade colorimetric sensing for glucose based on the H_2O_2 reaction has attracted the attention of researchers. Considering the highly specific peroxidase activity of Au/UiO-66 nanocomposites, it is likely to provide a highly selective method for the fast and convenient detection of glucose. Inspired by this idea, a cascade system was designed and established, as shown in Fig. 7a. Under a constant concentration of TMB, the oxidation degree mainly depends on the content of Au/UiO-66 and H_2O_2. Here the concentration of Au/UiO-66 was set as 50 μg mL^{-1}, the oxidation degree of TMB variation with H_2O_2 concentration is characterized. The standard curve of ΔA and glucose concentration was established by using the change of absorbance at 650 nm. In the range of 0.1–0.67 mM glucose concentration, the curve showed a good linear relationship ($R^2 = 0.997$), and the limit of detection (LOD) was calculated to be 0.033 mM (S/N = 3) (Fig. 7b and c). The absorbance of oxidized TMB (oxTMB) at 650 nm was evidently enhanced with the increase of H_2O_2, which was generated from glucose decomposition. Moreover, in order to evaluate the specificity of the colorimetric method, a series of control experiments were carried out, including different substrates such as galactose, fructose, maltose and sucrose. The concentration of all control substrates was set as 5 times that of glucose (20 mM). It appears that the absorption peak in glucose is dramatically higher than that in other substrates, exhibiting good specificity (Fig. 7d). We compared the data in Fig. 7d with the corresponding results of previous work (Pt/UiO-66).[48] It should be noted that when the amount of catalyst added was 0.1 mM, the signal to noise ratio (SNR) of Au/UiO-66 was 14.38 times as that of Pt/UiO-66. Furthermore, taking the interferents into consideration, the detecting specificity of Au/UiO-66 was about 3.2 times higher than that of Pt/UiO-66 in glucose detection (Fig. S5, ESI†). It could be explained that although the peroxidase-like activity of Au/UiO-66 is lower than that of Pt/UiO-66, Au/UiO-66 has almost no oxidase-like activity. This means that Au/UiO-66 has an extremely low interference background in the TMB color reaction, resulting in high detection sensitivity. However, Pt/UiO-66 has relatively strong oxidase-like activity, which may directly oxidize TMB and cause a high interference background during detection.

In addition, based on the remarkable peroxidase activity of Au/UiO-66 and the inhibitory effect of biomolecules on peroxidase activity, detection methods for dopamine and HS$^-$ were also developed. When dopamine is present in the reaction system, the amino and phenolic hydroxyl groups of dopamine could consume H_2O_2 through a reduction reaction, producing dopamine-o-quinine. As a result, less H_2O_2 would participate in the oxidation of TMB, resulting in the reduction of absorbance at 650 nm. Here the concentrations of Au/UiO-66, H_2O_2 and TMB were set to be constant and the influence of dopamine concentration on the oxidation degree of TMB was explored. With the increasing concentration of dopamine, the absorbance of the reaction system at 650 nm gradually decreased, indicating
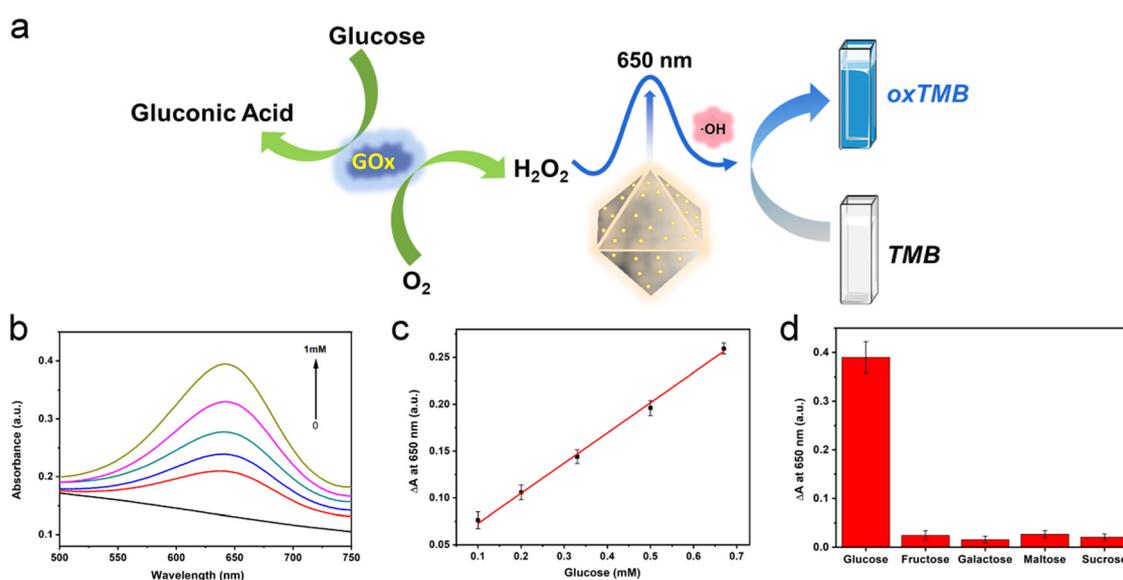

Fig. 7 (a) A schematic diagram of detection for glucose using Au/UiO-66. (b) Evolution of UV-Vis absorption spectra with increasing glucose concentration. (c) The standard curve of ΔA at 650 nm with increasing glucose concentration. (d) Selectivity of the glucose detection method.
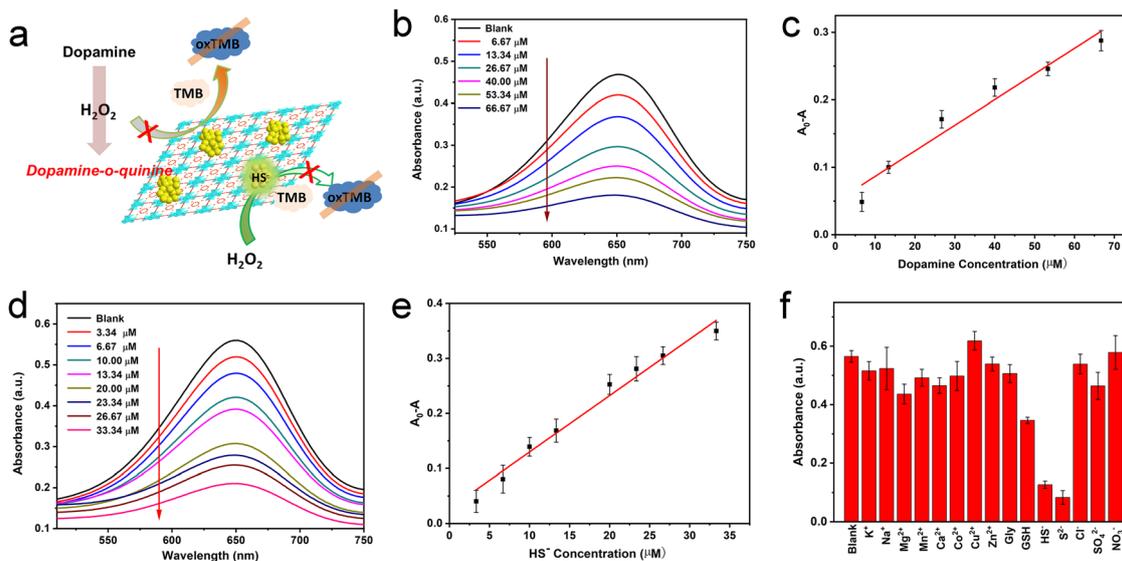
Fig. 8 (a) A schematic diagram of detection for dopamine and HS⁻ applied Au/UiO-66. (b) Evolution of UV-Vis absorption spectra with increasing dopamine concentration. (c) The standard curve of ΔA at 650 nm with increasing dopamine concentration. (d) Evolution of UV-Vis absorption spectra with increasing HS⁻ concentration. (e) A standard curve of ΔA at 650 nm with increasing HS⁻ concentration. (f) The selectivity of the HS⁻ detection method.

that H_2O_2 was gradually consumed (Fig. 8b). The standard curve of A_0–A (ΔA) with dopamine concentration was established, as shown in Fig. 8c. In the concentration range of 6.67–66.67 μM, the curve shows a good linear relationship ($R^2 = 0.95795$). The limit of detection (LOD) could reach 0.0022 mM (S/N = 3) (Fig. 8c).

Since H_2S is a weak acid, about 80% of H_2S exists as a single anion (HS⁻) under physiological conditions. HS⁻ is a highly reactive anion and more easily oxidized than H_2S.[54,55] HS⁻ has been reported to chemically bind with metal ions in the active part of horseradish peroxidase (HRP), which may poison the active surface of the noble metal NPs by metal–sulfur bonding and reduce their catalytic activity.[56] Thus, HS⁻ is likely to inhibit the catalytic oxidation of TMB by binding with Au NPs and reducing the peroxidase-like activity of the Au/UiO-66 nanocomposites.

Based on such an inhibiting mechanism, a colorimetric method for HS⁻ detection was developed. Analogously, the concentrations of Au/UiO-66, H_2O_2 and TMB were constant and the HS⁻ concentration was designed as the individual variable. Experimental results show that the oxidation degree of TMB significantly dropped with the increase of HS⁻ concentration (Fig. 8d). The standard curve of A_0–A (ΔA) with HS⁻ concentration was established. In the concentration range of 3.34–33.34 μM, the curve shows a good linear relationship ($R^2 = 0.97597$). The detection limit (LOD) was verified to be 0.0016 mM (Fig. 8e). Some common metal ions K⁺, Na⁺, Mg²⁺, Mn²⁺, Ni⁺, Co²⁺, Zn²⁺, Cu²⁺ and Ca²⁺ and sulfur-containing amino acids glycine (Gly), glutathione (GSH) and S²⁻ in biological systems were selected to evaluate the selectivity of the above method. The concentration of cationic interference substrate was 10 mM, which was five times higher than that of HS⁻, and the concentrations of glycine, GSH and S²⁻ were the same as HS⁻. According to the test results, little interference of other metal ions on the HS⁻

detection was observed expect for S²⁻, which may poison the Au NPs by a coating effect and reduce its catalytic activity, with just the same mechanism as HS⁻ (Fig. 8f).

4. Conclusions

In summary, the Au/UiO-66 composite nanozyme was synthesized by impregnation and a chemical reduction method. Au NPs with an average particle size of 7 nm were successfully loaded and uniformly distributed on UiO-66. The Au/UiO-66 exhibited remarkable peroxidase-like catalytic activity and insignificant oxidase-like activity, which makes it suitable for the detection of biological molecules. Therefore, a multi-targeted detecting platform was designed and established based on the outstanding peroxidase-like activity and good catalytic stability of Au/UiO-66. Experimental results show that the developed detection platform has the advantages of a simple procedure, high efficiency and good specificity. Meanwhile, it successfully realized multi-targeted detection of three different biomolecules (glucose, dopamine and HS⁻) and probably has high application potential and value in biological detection field.

Conflicts of interest

The authors declare no competing financial interests.

Acknowledgements

References

1 S. Ray, R. Biswas, R. Banerjee and P. Biswas, *Nanoscale Adv.*, 2020, **2**, 734–745.

2 C. Depre, J.-L. J. Vanoverschelde and H. Taegtmeyer, *Circulation*, 1999, **99**, 578–588.

3 D. Benton and D. S. Owens, *Psychopharmacology*, 1993, **113**, 83–88.

4 A. L. Galant, R. C. Kaufman and J. D. Wilson, *Food Chem.*, 2015, **188**, 149–160.

5 L. H. Fu, C. Qi, J. Lin and P. Huang, *Chem. Soc. Rev.*, 2018, **47**, 6454–6472.

6 R. A. Wise and M. A. Robble, *Annu. Rev. Psychol.*, 2020, **71**, 79–106.

7 T. M. Dawson and V. L. Dawson, *Science*, 2003, **302**, 819–822.

8 S. Latif, M. Jahangeer, D. Maknoon Razia, M. Ashiq, A. Ghaffar, M. Akram, A. El Allam, A. Bouyahya, L. Garipova, M. Ali Shariati, M. Thiruvengadam and M. Azam Ansari, *Clin. Chim. Acta*, 2021, **522**, 114–126.

9 C. J. Hong, H. C. Liu, T. Y. Liu, D. L. Liao and S. J. Tsai, *J. Neural Transm.*, 2005, **112**, 1503–1510.

10 G. K. Kolluru, X. Shen, S. C. Bir and C. G. Kevil, *Nitric oxide*, 2013, **35**, 5–20.

11 N. Tyagi, K. S. Moshal, U. Sen, T. P. Vacek, M. Kumar, W. M. Hughes, Jr., S. Kundu and S. C. Tyagi, *Antioxid. Redox Signaling*, 2009, **11**, 25–33.

12 K. Sasakura, K. Hanaoka, N. Shibuya, Y. Mikami, Y. Kimura, T. Komatsu, T. Ueno, T. Terai, H. Kimura and T. Nagano, *J. Am. Chem. Soc.*, 2011, **133**, 18003–18005.

13 H. Peng, Y. Cheng, C. Dai, A. L. King, B. L. Predmore, D. J. Lefer and B. Wang, *Angew. Chem., Int. Ed.*, 2011, **50**, 9672–9675.

14 H. J. M. N. Kimura, *Mol. Neurobiol.*, 2007, **26**, 13–19.

15 M. Ishigami, K. Hiraki, K. Umemura, Y. Ogasawara, K. Ishii and H. Kimura, *Antioxid. Redox Signaling*, 2009, **112**, 205–214.

16 W. Zhou, X. Gao, D. Liu and X. Chen, *Chem. Rev.*, 2015, **115**, 10575–10636.

17 M. Ganguly, C. Mondal, J. Jana, A. Pal and T. Pal, *Langmuir*, 2014, **30**, 4120–4128.

18 L. Zhang, L. Ning, S. B. Li, H. J. Pang, Z. F. Zhang, H. Y. Ma and H. Yan, *RSC Adv.*, 2016, **6**, 66468–66476.

19 Z. Guo, M. L. Seol, M. S. Kim, J. H. Ahn, Y. K. Choi, J. H. Liu and X. J. Huang, *Analyst*, 2013, **138**, 2683–2690.

20 J. Wu, X. Wang, Q. Wang, Z. Lou, S. Li, Y. Zhu, L. Qin and H. Wei, *Chem. Soc. Rev.*, 2019, **48**, 1004–1076.

21 L. Z. Gao, J. Zhuang, L. Nie, J. B. Zhang, Y. Zhang, N. Gu, T. H. Wang, J. Feng, D. L. Yang, S. Perrett and X. Y. Yan, *Nat. Nanotechnol.*, 2007, **2**, 577–583.

22 H. Wei, L. Gao, K. Fan, J. Liu, J. He, X. Qu, S. Dong, E. Wang and X. Yan, *Nano Today*, 2021, **40**, 101269.

23 R. F. Zhang, X. Y. Yan and K. L. Fan, *Acc. Mater. Res.*, 2021, **2**, 534–547.

24 D. M. Zhu, H. Chen, C. Y. Huang, G. X. Li, X. Wang, W. Jiang and K. L. Fan, *Adv. Funct. Mater.*, 2022, **32**, 2110269.

25 S. Zhang, R. F. Zhang, X. Y. Yan and K. L. Fan, *Small*, 2022, **18**, e2202294.

26 D. M. Zhu, M. Lyu, Q. Q. Huang, M. Suo, Y. Liu, W. Jiang, Y. H. Duo and K. L. Fan, *ACS Appl. Mater. Interfaces*, 2020, **12**, 36928–36937.

27 J. Yang, R. F. Zhang, H. Q. Zhao, H. F. Qi, J. Y. Li, J. F. Li, X. Y. Zhou, A. Q. Wang, K. L. Fan, X. Y. Yan and T. Zhang, *Exploration*, 2022, **2**, 20210267.

28 X. Li, H. J. Zhu, P. Liu, M. Z. Wang, J. M. Pan, F. X. Qiu, L. Ni and X. H. Niu, *Trends Anal. Chem.*, 2021, **143**, 116379.

29 S. R. Li, Y. H. Zhang, Q. Wang, A. Q. Lin and H. Wei, *Anal. Chem.*, 2021, **94**, 312–323.

30 J. Golchin, K. Golchin, N. Alidadian, S. Ghaderi, S. Eslamkhah, M. Eslamkhah and A. Akbarzadeh, *Artif. Cells, Nanomed., Biotechnol.*, 2017, **45**, 1–8.

31 H. Wang, K. W. Wan and X. H. Shi, *Adv. Mater.*, 2019, **31**, e1805368.

32 Q. W. Liu, A. M. Zhang, R. H. Wang, Q. Zhang and D. X. Cui, *Nano-Micro Lett.*, 2021, **13**, 154.

33 W. Zhang, J. L. Dong, Y. Wu, P. Cao, L. N. Song, M. Ma, N. Gu and Y. Zhang, *Colloids Surf., B*, 2017, **154**, 55–62.

34 Y. H. Peng, Z. Y. Wang, W. S. Liu, H. L. Zhang, W. Zuo, H. A. Tang, F. J. Chen and B. D. Wang, *Dalton Trans.*, 2015, **44**, 12871–12877.

35 S. W. Cao, F. F. Tao, Y. Tang, Y. Li and J. G. Yu, *Chem. Soc. Rev.*, 2016, **45**, 4747–4765.

36 S. Liang, X. L. Wu, J. Xiong, M. H. Zong and W. Y. Lou, *Coord. Chem. Rev.*, 2020, **406**, 213149.

37 L. Jiao, J. Wang and H. L. Jiang, *Acc. Mater. Res.*, 2021, **2**, 327–339.

38 C. H. Fu, H. Q. Zhou, L. F. Tan, Z. B. Huang, Q. Wu, X. L. Ren, J. Ren and X. W. Meng, *ACS Nano*, 2018, **12**, 2201–2210.

39 W. C. Hu, M. R. Younis, Y. Zhou, C. Wang and X. H. Xia, *Small*, 2020, **16**, 2000553.

40 X. Liu, W. Qi, Y. F. Wang, R. X. Su and Z. M. He, *Eur. J. Inorg. Chem.*, 2018, 4579–4585.

41 A. Loosen, C. Simms, S. Smolders, D. E. De Vos and T. N. Parac-Vogt, *ACS Appl. Nano Mater.*, 2021, **4**, 5748–5757.

42 H. G. T. Ly, G. Fu, F. de Azambuja, D. De Vos and T. N. Parac-Vogt, *ACS Appl. Nano Mater.*, 2020, **3**, 8931–8938.

43 N. Kruse and S. Chenakin, *Appl. Catal., A*, 2011, **391**, 367–376.

44 A. Zwijnenburg, A. Goossens, W. G. Sloof, M. W. J. Crajé, A. M. van der Kraan, L. Jos de Jongh, M. Makkee and J. A. Moulijn, *J. Phys. Chem. B*, 2002, **106**, 9853–9862.

45 E. Irissou, M.-C. Denis, M. Chaker and D. Guay, *Thin Solid Films*, 2005, **472**, 49–57.

46 W. W. He, Y. Liu, J. S. Yuan, J. J. Yin, X. C. Wu, X. N. Hu, K. Zhang, J. B. Liu, C. Y. Chen, Y. L. Ji and Y. T. Guo, *Biomaterials*, 2011, **32**, 1139–1147.

47 T. Wen, W. W. He, Y. Chong, Y. Liu, J. J. Yin and X. C. Wu, *Phys. Chem. Chem. Phys.*, 2015, **17**, 24937–24943.

48 H. H. Wang, J. Zhao, C. Liu, Y. P. Tong and W. W. He, *ACS Omega*, 2021, **6**, 4807–4815.

49 M. Sharifi, K. Faryabi, A. J. Talaei, M. S. Shekha, M. Ale-Ebrahim, A. Salihi, N. M. Q. Nanakali, F. M. Aziz, B. Rasti, A. Hasan and M. Falahati, *J. Mol. Liq.*, 2020, **297**, 112004.

50 L. M. M. Tijskens, R. Greiner, E. S. A. Biekman and U. Konietzny, *Biopolymers*, 2000, **72**, 323–330.

51 G. Rabai, K. Kustin and I. R. Epstein, *J. Am. Chem. Soc.*, 1989, **111**, 3870–3874.

52 S. Strbac, *Electrochim. Acta*, 2011, **56**, 1597–1604.

53 W. W. He, Y. T. Zhou, W. G. Wamer, X. N. Hu, X. C. Wu, Z. Zheng, M. D. Boudreau and J. J. Yin, *Biomaterials*, 2013, **34**, 765–773.

54 M. D. Hartle and M. D. Pluth, *Chem. Soc. Rev.*, 2016, **45**, 6108–6117.

55 N. Lau, L. N. Zakharov and M. D. Pluth, *Chem. Commun.*, 2018, **54**, 2337–2340.

56 W. W. He, X. N. Han, H. M. Jia, J. H. Cai, Y. L. Zhou and Z. Zheng, *Sci. Rep.*, 2017, **7**, 40103.